DOI: 10.1002/chem.200500040

# Surface-Grafted Multiporphyrin Arrays as Light-Harvesting Antennae to Amplify Photocurrent Generation

**Mitsuhiko Morisue, Shigeru Yamatsu, Noriko Haruta, and Yoshiaki Kobuke*[a]**

**Abstract:** Organized multiporphyrin arrays were developed on the conductive surface by a novel coordination-directed molecular architecture aiming at efficient photoelectric conversion. The basic strategy employs the mutual coordination of two imidazolylporphyrinatozinc(II) units to form a cofacial dimer. Thus, *meso*,*meso*-linked bis(imidazolylporphyrinatozinc) ($Zn_2(ImP)_2$) was organized onto imidazolylporphyrinatozinc on the gold substrate as a self-assembled monolayer. The organized $Zn_2(ImP)_2$ bearing allyl side chains was covalently linked by ring-closing olefin metathesis catalyzed with Grubbs catalyst. Alternating coordination/metathesis reactions allow the stepwise accumulation of multiporphyrin arrays on the gold electrode. A successive increase in absorption over a wide wavelength range occurred after each accumulation step of $Zn_2(ImP)_2$ on the gold electrode, and cathodic photocurrent generation was enhanced in the aqueous electrolyte system, containing viologen as an electron carrier. The significant increase of the photocurrent indicates that the multiporphyrin array works as a "light-harvesting antenna" on the gold electrode.

**Keywords:** interfaces · molecular devices · porphyrinoids · self-assembly · zinc

## Introduction

Spontaneous molecular assembly on solid surfaces is a key technique in engineering molecular-based devices. Particularly, the field of photoenergy conversion systems is an area of most intense research. In the development of such molecular systems, well-arranged redox species are prerequisite in controlling interfacial electron transport.[1] For this purpose, various surface-fabrication methods have been applied for alignment, for example, Langmuir–Blodgett (LB) films,[2] self-assembled monolayers (SAMs),[3] or layer-by-layer membranes.[4] These systems performed successfully as simplified models for the primary process in photosynthesis. Molecular systems for efficient artificial "light-harvesting" photoenergy conversion have been constructed based on the design by Fujihira and co-workers.[2e] These were accomplished by funneling the photoexcitation energy on the antenna molecules into a donor–sensitizer–acceptor triad by lateral energy transfer within the monolayer assemblies.[2e,3f,3h] To mimick a natural "light-harvesting" function, it is important to capture solar light over a wide wavelength range as well as to mediate excitation-energy transport. The small extinction of the monomolecular layers has been overcome by employing porous nanocrystalline electrodes in Grätzel's dye-sensitizing solar cell.[5]

The present paper proposes another type of molecular architecture in fabricating multiporphyrin assemblies with increased extinction. Metal–ligand interaction is a powerful tool to build structurally regular multilayered assemblies on conductive surfaces.[6] Besides, the fully conjugated metal complexes may enhance electronic and optical communications among the individual layer constituents. The porphyrin macrocycle is the fundamental chromophore framework in natural photosynthetic systems, in which the special pair collects solar energy from the peripheral light-harvesting antennae with excellent yields.[7] Hence, considerable attention is now focused on developing photoelectronic devices using electrodes with porphyrins attached. Axial coordination of metalloporphyrin has been exploited as a building tool to immobilize porphyrins at conductive surfaces.[8]

For tailoring extremely long multiporphyrin arrays, we have focused on a self-organization methodology utilizing imidazolylporphyrinatozinc(II) units. Two such units mutually coordinate through imidazolyl groups attached to the central zinc atom to form a cofacial dimeric structure, which can also serve as a precise motif of the unit structure that

[a] Dr. M. Morisue, S. Yamatsu, N. Haruta, Prof. Y. Kobuke
Graduate School of Materials Science
Nara Institute of Science and Technology
8916–5 Takayama, Ikoma, Nara 630–0101 (Japan)
Fax: (+81) 743-72-6119
E-mail: kobuke@ms.naist.jp

Supporting information for this article is available on the WWW under http://www.chemeurj.org/ or from the author.

  

constitutes the bacterial light-harvesting antenna system.[9,10] Bis(imidazolylporphyrinatozinc(II)) units spontaneously assemble into multiporphyrin arrays in isotropic media[11] and even at the electrode surface modified with imidazolylporphyrinatozinc as a SAM.[12] The cofacial dimer in a van der Waals contact shows exciton coupling indicative of strong ground-state electronic interactions and therefore delocalizes photoexcited energy or a photogenerated hole in the coordination dimer. Its continuous link is also an excellent energy/electron/hole-transferral agent. The porphyrin wires can be developed noncovalently by successive coordination-dimer formation. The multiporphyrin array assembled on the gold electrode was further modified to generate a large photocurrent.[12a]

Covalent immobilization of the organized porphyrin will produce advantages in the structural stability and in the molecular arrangement of the multiporphyrin array. The coordination dimer unit of imidazolylporphyrin with allyl-substituents can be connected to each other by a ring-closing olefin metathesis reaction catalyzed with Grubbs catalyst (a ruthenium–carbene complex).[13,14] The metathesis reaction quantitatively proceeds under mild conditions. The covalently linked cofacial dimer structures remain even in pyridine due to the extremely large stability constant of the complementary coordination.[14a] We attempted stepwise immobilization of the imidazolylporphyrinatozinc complexes to construct heterogeneous multiporphyrin arrays on the imidazolylporphyrinatozinc–SAM-modified gold electrode (see Scheme 1). The photocurrent was therefore enhanced by efficient light excitation through large extinction—the so-called "light-harvesting antenna" function.

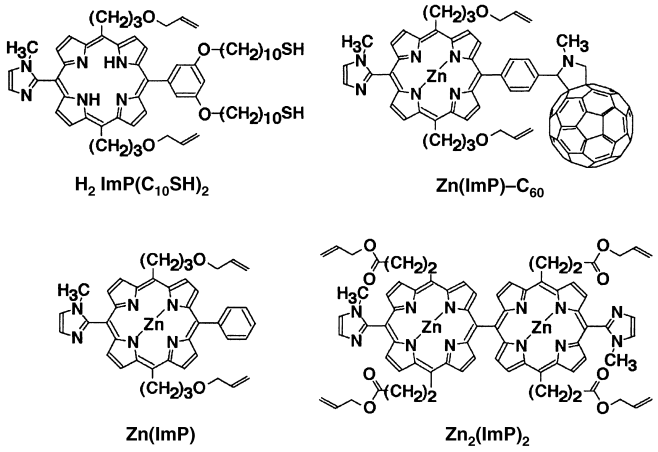


## Results and Discussion

**Formation of a SAM incorporating imidazolylporphyrin**: The first layer of imidazolylporphyrinatozinc was deposited on the gold surface as a SAM. The gold substrate was soaked in a solution of $H_2ImP(C_{10}SH)_2$ in $CH_2Cl_2$ (0.5 mM) for 20 h (step i) in Scheme 1). After immersion, the substrate was rinsed thoroughly with $CH_2Cl_2$ and then dried under a stream of nitrogen. Zinc(II) was introduced to the free-base imidazolylporphyrin by gentle reflux for 2 h under a nitrogen atmosphere in chloroform containing a small amount of saturated zinc acetate in methanol (step ii) in Scheme 1). The Soret band at 421 nm shifted to 428 nm, and the Q-band at 516 nm, attributed to free-base porphyrin, changed to 550 nm, indicating that zinc was introduced as the central metal ion in the monolayer assemblies (Figure 1). The characteristic oxidation peak of porphyrinatozinc also appeared around 680 mV in the cyclic voltammogram for the SAM on the gold electrode (see Figure 11b later in the text).

Surface concentration can be determined by means of electrochemical desorption, a method well-established by Porter and co-workers.[15] The one-electron reductive desorption under alkaline conditions (pH > 11) is a direct method of observing the Au–S covalent-bond cleavage. The cyclic voltammogram of the porphyrinatozinc SAM in KOH (0.5 M) showed irreversible reduction peaks at −1069 mV versus Ag/AgCl at 100 mV s$^{-1}$ scan rate (Figure 2). The reduction waves were assigned to the reductive cleavage of the Au–S covalent bond. In agreement with this assignment, this peak gradually diminished in the course of potential sweep cycles. The integrated current gives the surface concentration of Au–S bonding, $\Gamma_T = (iV)/(ve)$, in which $i$, $V$, $v$, and $e$ denote current density, potential, sweep-rate, and elemental charge, respectively. The surface coverage of the imidazolylporphyrinatozinc complex ($\Gamma_T/2$) is therefore calculated as $1.35 \times 10^{13}$ mol cm$^{-2}$, corresponding to the molecular area of 7.4 nm$^2$ molecule$^{-1}$.

The SAM was also characterized by using $[Fe(CN)_6]^{3-}$ as a bulk redox probe.[16] The electrode surface covered with the SAM was completely insulated from the bulk ferricyanide species, even after the zinc insertion (Figure 3b). The imidazolylporphyrinatozinc complexes were thus assumed to form a stable SAM on the gold surface.

**Stepwise accumulation of surface-grafted multiporphyrin arrays**: The SAM-modified gold substrate was immersed for 1 h in $Zn_2(ImP)_2$ (1 mM) in $CH_2Cl_2$ with methanol (20 equiv) as coordinating solvent to partially dissociate the otherwise extensively developed coordination. This was followed by rinsing with $CH_2Cl_2$ to organize the imidazolyl-to-zinc coordination by removal of methanol (step iii) in Scheme 1). The organized $Zn_2(ImP)_2$ was covalently immobilized through metathesis reactions of allyl groups by soaking for 10 min in a dilute solution of Grubbs catalyst in $CH_2Cl_2$ (step iv) in Scheme 1).[17] The gold substrate was thoroughly washed successively with a large excess of $CH_2Cl_2$, methanol, and water, and then dried under a stream of nitrogen.

Absorption spectra of species on the gold substrate demonstrate the difference of coordination behavior of $Zn_2(ImP)_2$ depending on the surface chemical species. Only a small amount of $Zn_2(ImP)_2$ can be adsorbed physically onto a bare gold substrate or octanethiol-SAM-modified substrate. For the Zn–porphyrin SAM or the $H_2$–porphyrin

  

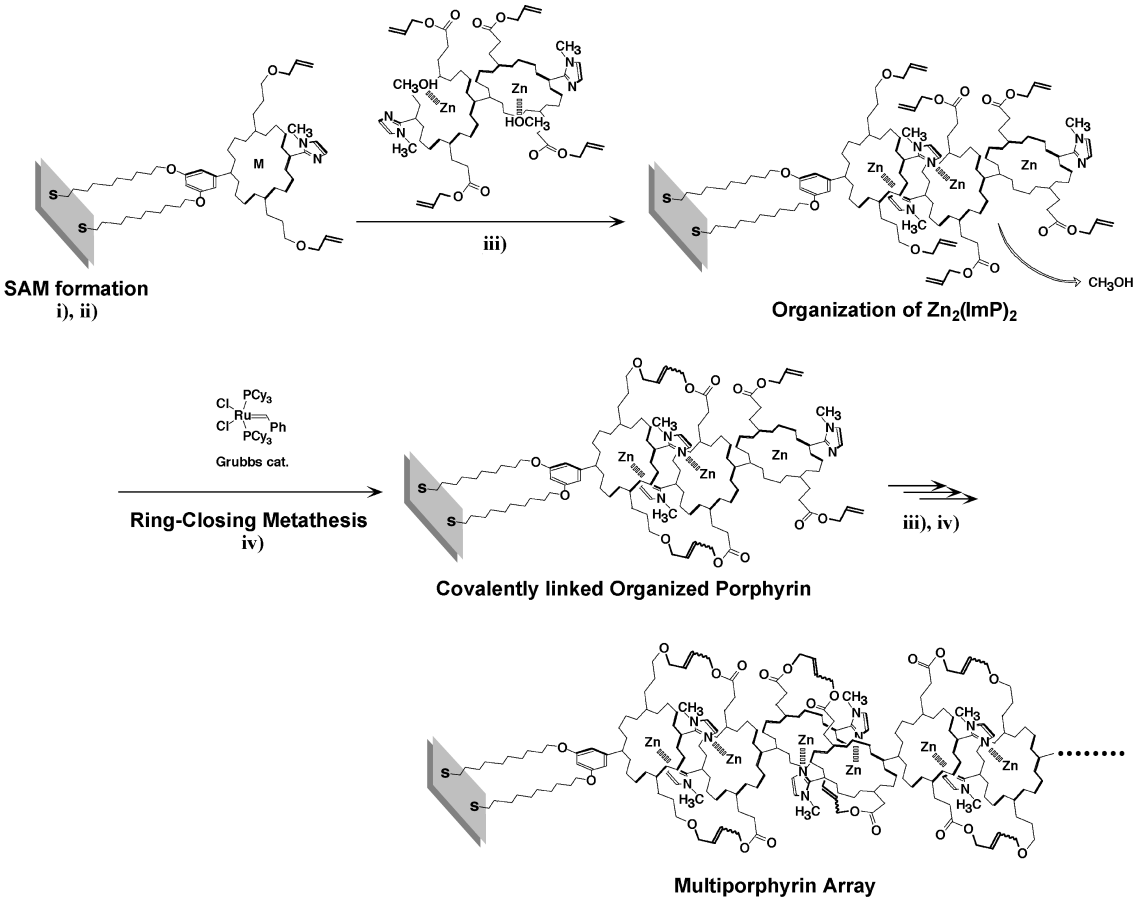


Scheme 1. Procedures for accumulation of the multiporphyrin arrays on the gold substrate. i) To form the SAM, the gold substrate was immersed in $H_2ImP(C_{10}SH)_2$ (0.1 mM in $CH_2Cl_2$) for 20 h. ii) Zinc was introduced into the porphyrin in the SAM in $CHCl_3$ containing a small amount of saturated $Zn(OAc)_2$ in MeOH at 50 °C for 2 h. iii) The SAM-modified gold was soaked with $Zn_2(ImP)_2$ (1 mM in $CH_2Cl_2$) containing MeOH (20 mM) at room temperature for 1 h, and then rinsed with $CH_2Cl_2$ to organize $Zn_2(ImP)_2$ by removal of MeOH. iv) The substrate was soaked in a dilute solution of Grubbs catalyst at room temperature for 10 min. The covalently linked organized porphyrin was obtained after thoroughly rinsing with MeOH and $CH_2Cl_2$. The repetition steps iii) and iv) provided the multiporphyrin array. The most plausible structure for intradimer metathesis is illustrated.

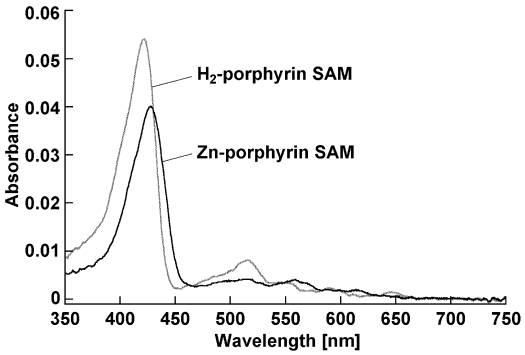


Figure 1. Absorption spectra of $H_2$– and Zn–porphyrin SAM on the gold electrode.

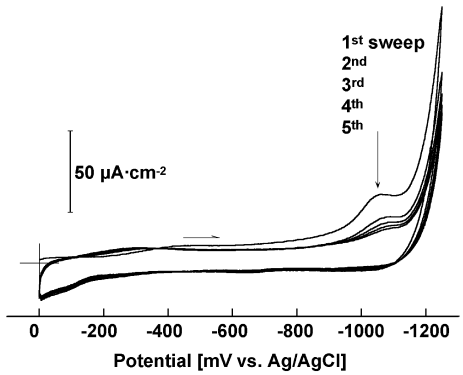


Figure 2. Cyclic voltammograms for the SAM-incorporated imidazolylporphyrinatozinc on the gold electrode. Conditions: KOH (0.5 M) supporting electrolyte in aqueous media under continuous nitrogen stream at a 100 mV $s^{-1}$ sweep rate. A Pt-wire electrode and a Ag/AgCl (saturated KCl) electrode were used as the counter and the reference electrode, respectively.

SAM, an apparently large increase of the absorbance was found around 480 nm, attributable to $Zn_2(ImP)_2$ (Figure 4). This comparison suggests that $Zn_2(ImP)_2$ is organized at the central zinc through complementary coordination with Zn–SAM or axial ligation to $Zn_2(ImP)_2$ on the $H_2$ SAM surface.

  

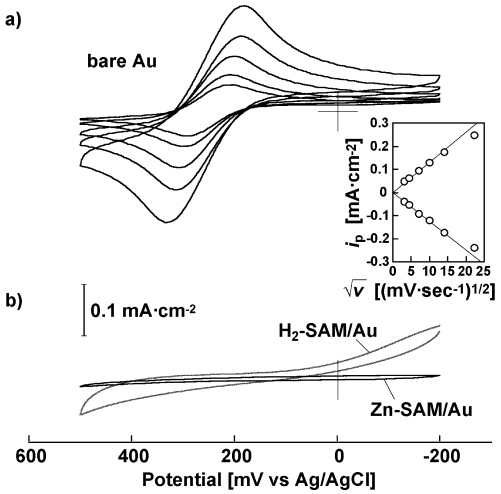


Figure 3. Cyclic voltammograms of $K_3Fe(CN)_6$ (1 mM) in $Na_2SO_4$ (0.1 M) electrolyte solution. a) Redox behavior observed for the bare Au working electrode at 10, 20, 50, 100, and 200 mV $s^{-1}$ and the proportional relation between the peak-current $i_p$ versus $v^{1/2}$ at $2.2\times10^{-18}$ $cm^2s^{-2}$ of the diffusion constant up to 100 mV $s^{-1}$ of the sweep rate (inset). b) The insulation of the redox of $K_3[Fe(CN)_6]$ (1 mM) for the SAM-attached working electrodes.

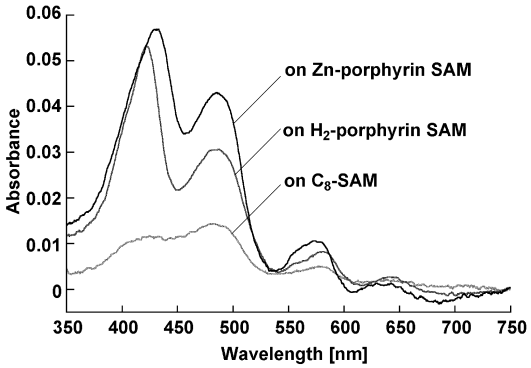


Figure 4. Absorption spectra of the SAM-modified gold substrate after soaking for 1 h in a solution of $Zn_2(ImP)_2$. The adsorbates forming the SAM are indicated in the figure.

The substrate that had been immersed in a solution of $Zn_2(ImP)_2$ over 2 h did not show further increase of the absorption in the subsequent cycles. Prolonged organization may bridge the imidazolylporphyrinatozinc terminals to prevent further coordination. These findings strongly suggest that the outer terminal was a critical factor for sequential deposition of $Zn_2(ImP)_2$ on the gold surface.

The organized $Zn_2(ImP)_2$ was then treated with Grubbs catalyst for ring-closing metathesis. Alternating treatment of the Zn–porphyrin SAM/Au substrate with a solution of $Zn_2(ImP)_2$ and Grubbs catalyst resulted in a gradual rise in the absorption at 480 nm up to 0.18 after six cycles in Figure 5a. The accumulation process requires dissociation and organization by addition and elimination, respectively, of the coordinating solvent, methanol, in the above treatment. The covalently immobilized, organized porphyrin cannot be dissociated by the addition of the coordinating solvent in each organization step. In contrast, the cumulative layering of $Zn_2(ImP)_2$ was difficult to control through noncovalent deposition. Without treatment with Grubbs catalyst, the first accumulation of $Zn_2(ImP)_2$ was observed, but no successive increase was observed by the repetition (Figure 5b). In a solution system, metathesis reaction of the allyl side chains shows high specificity of the spacer chain length for the covalent linkage of the complementary porphyrin dimer.[14a] Since the optimum spacer to give a 95% yield in solution was utilized in the present system, the dimer connection must occur efficiently on the gold substrate. In the present case, however, interarray cross-linking may also occur to a greater or lesser extent and contribute to the stabilization of the multiporphyrin arrays. Both the complementary coordination through imidazolyl-to-zinc and covalent linking of the allyl side chains are indispensable for the successive accumulation of multiporphyrin arrays.

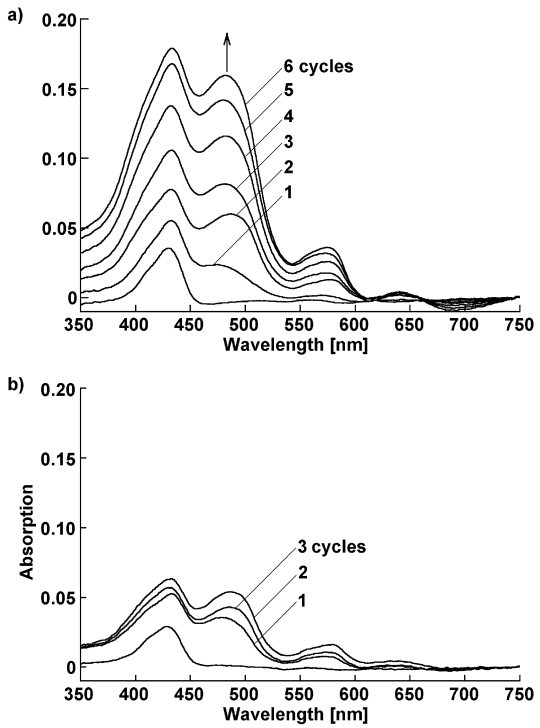


Figure 5. Effect of the metathesis reaction on the growth of $Zn_2(ImP)_2$ on the imidazolylporphyrinatozinc SAM/Au substrate. a) The substrate treated with alternate cycles of coordination organization/metathesis reactions. The spectrum was recorded after every metathesis reaction. b) The substrate dipped repetitively in a solution of $Zn_2(ImP)_2$ without metathesis.

The average thickness of the multiporphyrin layer on the gold was evaluated by the surface plasmon resonance (SPR) angles in water. The incident angle increased as a function of the accumulation cycles. Based on the Fresnel's fittings, a layer with a thickness of approximately 0.9–1.2 nm grew in a single accumulation cycle (Figure 6). The porphyrin should interdigitate with the Zn–porphyrin terminal to be accumulated at the surface. The distance from the terminal imidazolyl edge to the neighboring imidazolyl edge was estimated

  

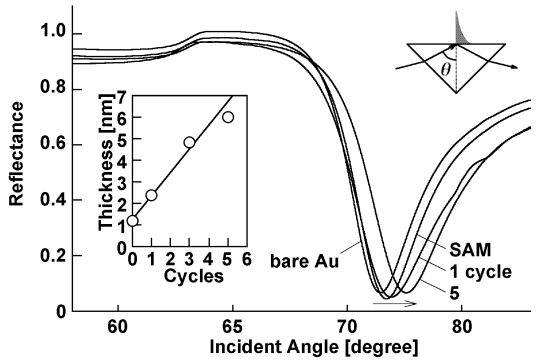


Figure 6. SPR angles of the multiporphyrin array on the gold substrate in water. The plot of the thickness as a function of the accumulation cycle (inset).

to be around 1.5 nm by the molecular mechanics calculation assuming complementary coordination (Figure 7). The surface-grafted multiporphyrin arrays are therefore assumed to be elongated by approximately a single $Zn_2(ImP)_2$ accumulation cycle.

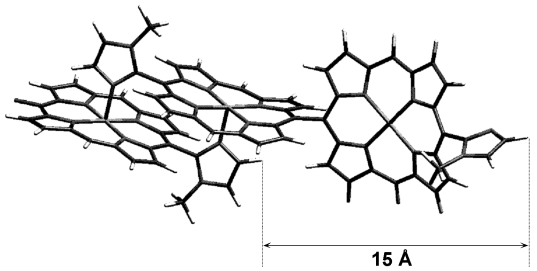


Figure 7. Molecular model of $Zn_2(ImP)_2$ coordinating with imidazolylporphyrinatozinc drawn by the molecular mechanics calculation software (Cerius 2 supplied by Accelrys, Ver. 4.6/Force Field UNIVERSAL 1.02). The view omits the allyl side chains for visual clarity.

The accumulated porphyrins were also observed by AFM. The topographic images in the present system showed no significant difference from those of the surface roughness of the vacuum-deposited gold AFM images (see Figure S2 in the Supporting Information). In the previous experiment, the porphyrins were organized by evaporating pyridine from nitrobenzene/pyridine (1:1 v/v), and were grown to a heterogeneous mixture of the multiporphyrin-like stalagmite.[12] The stepwise coordination/metathesis can thus regulate the gradual elongation of the porphyrin on the whole area of the gold substrate.

**Photocurrent generation by multiporphyrin antennae**: We measured the photocurrent response in the presence of viologen as an electron carrier by varying the applied potential for the sample after several accumulation cycles. Prompt response was maintained as stable without detectable change of the photocurrent over several hours for the experimental operation. Figure 8 depicts typical photocurrent response patterns during on–off cycles of white light at a potential

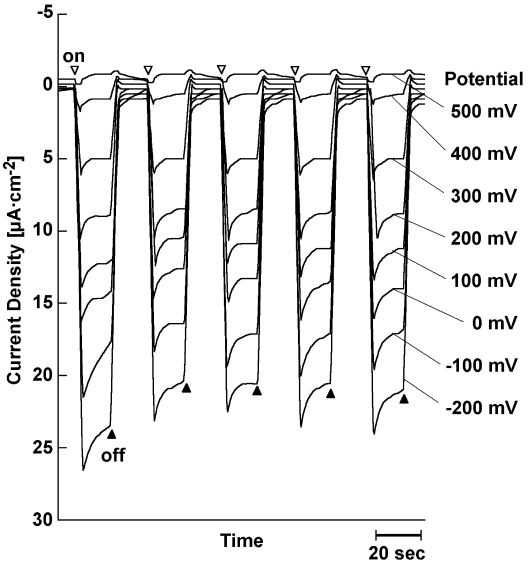


Figure 8. Photoresponse patterns during on/off cycles of white light at various potentials. Conditions: $Na_2SO_4$ (0.1 M) supporting electrolyte and methylviologen (10 mM) electron-carrier in the aqueous system under nitrogen streaming. The $Zn_2(ImP)_2$ was accumulated over four deposition cycles.

range of 500 to −200 mV versus Ag/AgCl. A steep rise and fall of the cathodic current was found as soon as the light was turned on and off, respectively. The photocurrent density gradually increased on applying a more negative potential. We observed only cathodic photocurrent for the viologen–multiporphyrin–Au combination. The photorectifying effect implies that most of the electrons flow unidirectionally from the photoexcited porphyrin to the bulk viologen. Furthermore, the cathodic photocurrent was amplified by the increased accumulation of the porphyrin antennae, keeping the dark current at the same level (Figure 9). The multiporphyrin array could increase the magnitude of the photocurrent depending on the degree of accumulation subduing the effect of distance elongation between two interfacial electron-transport sites.

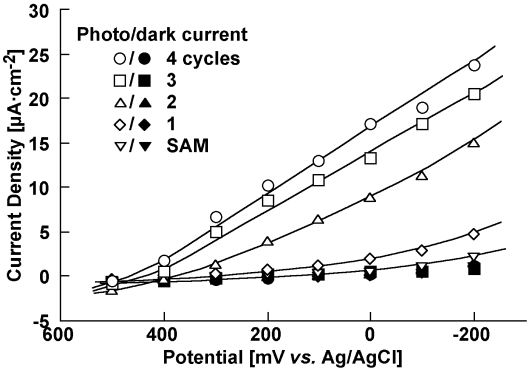


Figure 9. Current-potential relationship for the dark and the photocurrent (white light irradiation).

  

The photocurrent-action spectra obtained were normalized to the illuminated light intensity at a constant value of 174.6 $\mu W\,cm^{-2}$. Close coincidence of these spectra with the corresponding absorption spectra (Figure 5a) proves that the photocurrent is generated by the photoexcitation of Zn–porphyrins (Figure 10). In addition, the accumulation of $Zn_2(ImP)_2$ induced a significant increase of the photocurrent generation. The increase of the photocurrent was small for the samples of the first two accumulation cycles, but became significant for the samples of the last three. This agrees with the observation that the excited singlet-state of Zn–porphyrin moieties is quenched strongly in the vicinity of the gold surface.[3j,18] Photoexcitation at metal surfaces generally accompanies energy-transfer quenching by surface plasmons. The imidazolylporphyrinatozinc SAM on the gold surface hardly fluoresces. Hence, the photoexcitation of the inner porphyrin contributed less to the photocurrent generation, whereas the inner porphyrin played a role in spacing the outer antennae from the gold surface in order to suppress the deactivation by surface plasmon and to mediate hole migration along the porphyrin array. The photosensitization was therefore enhanced by the accumulation of $Zn_2(ImP)_2$. Photocurrent augmentation at 480 nm and the Q-bands was larger than the increase at 430 nm, while the ratio of accumulated absorbance did not change very much. This was in line with a greater contribution of the Soret band around 480 nm and the Q-bands to fluorescence in $CH_2Cl_2$ (see Figure S1 in the Supporting Information). Successive accumulation therefore provided improvement in photocurrent generation particularly sensitized by light excitation at longer wavelengths.

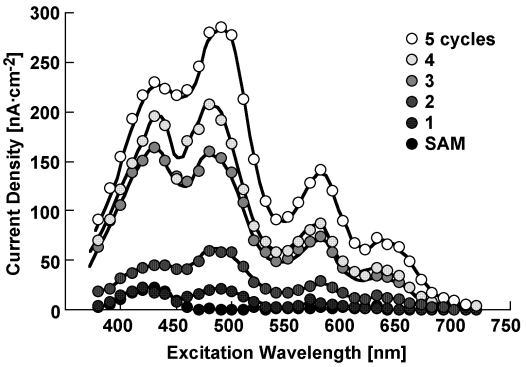


Figure 10. Photocurrent-action spectra of the multiporphyrin on the gold electrode at −200 mV versus Ag/AgCl. The spectra were normalized to a constant light intensity at 174.6 $\mu W\,cm^{-2}$.

The photocurrent generation can be composed of the following multi-elementary steps 1–10

Photoexcitation : $P + h\nu \rightarrow P^*$ (1)

Energy migration : $P^* + P \rightarrow P + P^*$ (2)

Hole migration : $P^{+\cdot} + P \rightarrow P + P^{+\cdot}$ (3)

Charge migration : $P^{-\cdot} + P \rightarrow P + P^{-\cdot}$ (4)

Redox reaction : $P^{+\cdot} + e^- \rightarrow P$ (5)

$P^* + e^- \rightarrow P^{-\cdot}$ (6)

Viologen reduction : $P^* + MV^{2+} \rightarrow P^{+\cdot} + MV^{+\cdot}$ (7)

$P^{-\cdot} + MV^{2+} \rightarrow P + MV^{+\cdot}$ (8)

Deactivation : $P^* + Au \rightarrow P + Au^*$ (9)

$P^{+\cdot} + P^{-\cdot} \rightarrow P + P$ (10)

The primary photoinduced charge separation proceeds between the excited porphyrin and bulk viologen as the electron acceptor [Eq. (7)]. The hole generated migrates towards the electrode surface [Eq. (3)] and receives an electron at negative potential to give the cathodic current [Eq. (5)]. The redox potentials were determined by cyclic voltammetry (Figure 11). Zn–porphyrin complexes on the Au electrode possess a broad oxidation potential due to hydrophobicity and electroinactivity within the densely packed porphyrin assemblies. The oxidation potential around 685 mV did not shift significantly with accumulation of $Zn_2(ImP)_2$. The redox potential of the Zn(ImP) unit in the SAM may shift from the monomeric state, because the Soret band showed a bathochromic shift suggesting J-type

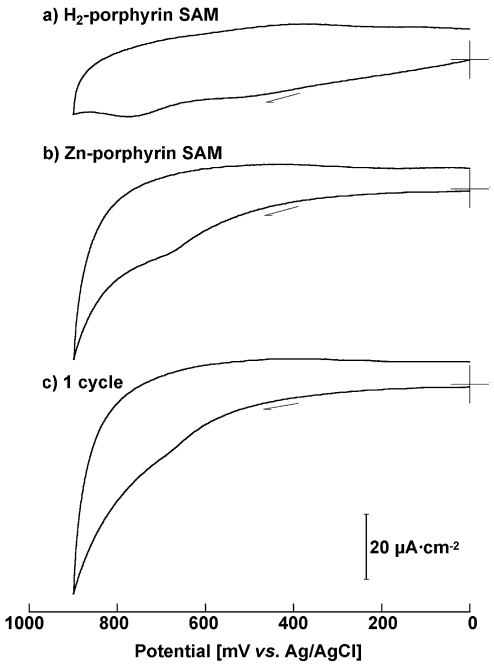


Figure 11. Cyclic voltammograms. a) $H_2$–porphyrin SAM on the gold electrode. b) Zn–porphyrin SAM. c) A multiporphyrin array (one-cycle deposition) on the gold electrode at 50 $mV\,s^{-1}$. Conditions: $Na_2SO_4$ (0.1 M) supporting electrolyte in the aqueous system under a nitrogen stream. Further accumulation did not increase the electrochemical response under the conditions.

  

aggregation in the SAM (Figure 1). We suppose that this is the reason for no significant shift of the redox potentials on the accumulation cycles of $Zn_2(ImP)_2$. Even though the oxidation potentials have a wide distribution, the overall charge and hole migration should proceed in a downhill direction as shown in Scheme 2, which depicts the dominant processes for the cathodic photocurrent generation.

An alternative mechanism may also account for the present photocurrent conversion system. If electron injection from the electrode to the excited porphyrin occurs at an early stage [Eq. (6)], the multiporphyrin array must mediate the excess charge [Eq. (4)] to reduce viologen in the bulk solution [Eq. (8)]. Although it is difficult to choose the most probable one from these two mechanisms, Equations (1),(7),(3),(5) and Equations (1),(6),(4),(8), the former mechanism seems to be more likely for the present system, because porphyrins generally act as *p*-type semiconductors.[19]

Regarding the photocurrent generation on the gold electrode, the energy migration process along the porphyrin arrays [Eq. (2)] should compete with quenching by surface plasmon [Eq. (9)] as noted previously. This should reduce the incident photon-to-current conversion efficiency (IPCE) value. Nevertheless, the IPCE value shows a sharp rise up to 0.4% at 480 nm as the light-harvesting efficiency ($LHE = 1-10^{-A}$, derived from Beer's law)[5a,20] increases (Figure 12). This value, observed for the flat electrode, is relatively large compared with the values (0.037% at 430 nm for the Zn–porphyrin SAM in the present system) conventionally observed for SAM systems.[3k]

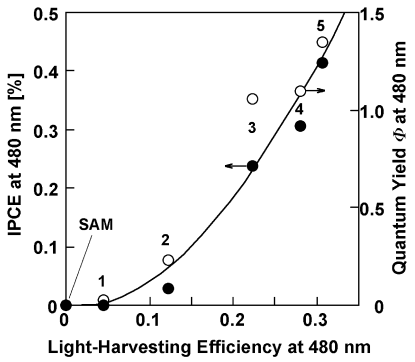


Figure 12. Plots for the IPCE (●) and quantum yield (○) against LHE at 480 nm at −200 mV (versus Ag/AgCl). The numbers in the Figure denote the deposition cycles.

The IPCE value is determined as Equation (11) follows:[5a,20]

$$\text{IPCE}\ (\%) = 100\,(i/e)/(W\lambda/hc) \tag{11}$$

in which $i$, $W$, and $\lambda$ are photocurrent density ($A\,cm^{-2}$), the incident photon flux ($174.6\times10^{-6}\,W\,cm^{-2}$), and wavelength (nm), respectively. At the same time, the IPCE value is related to the LHE and the quantum efficiency $\Phi$ after light absorption by Equation (12).

$$\Phi\ (\%) = \text{IPCE}/\text{LHE} \tag{12}$$

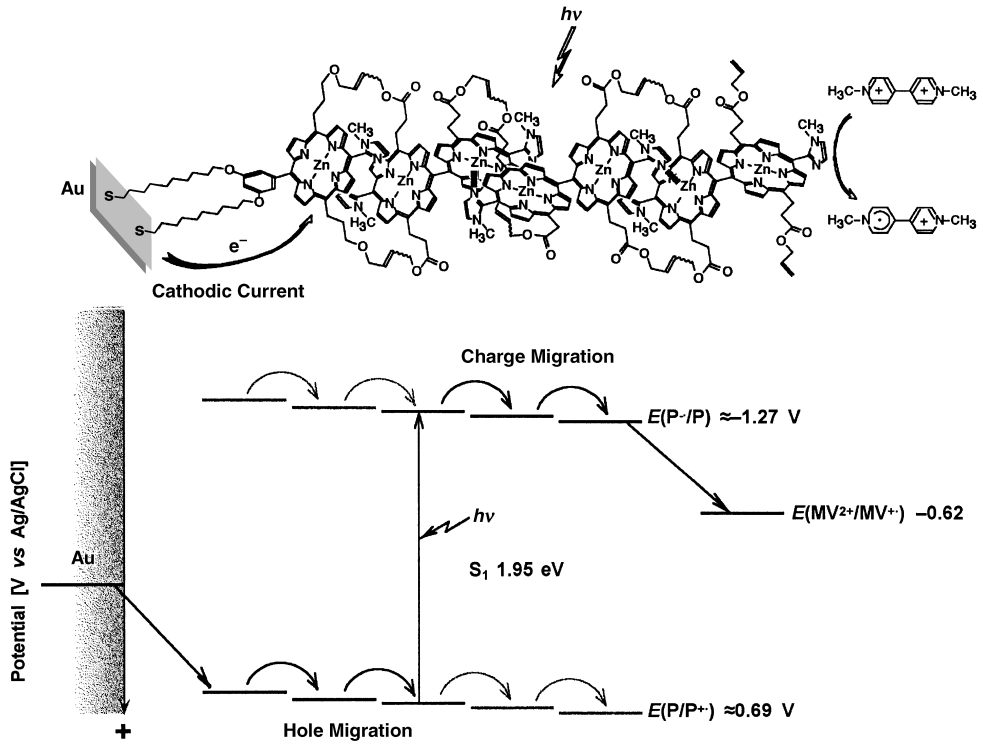


Scheme 2. Potential diagram for photoinduced charge-separation steps. The recombination processes, energy-transfer process, and distributed potentials without contribution to photocurrent generation are omitted for simplification.

  

The plot of $\Phi$ against LHE at 480 nm also shows a sharp increase as LHE increases (Figure 12, right-hand axis). This means that the accumulation of $Zn_2(ImP)_2$ is effective not only for light absorption, but also for generation of the electric current.

The above evaluation may be extended to all the absorption wavelengths. The results shown in Figure 10 demonstrate that efficient light-to-current conversion is due to light-capture over a wide range of wavelengths. The "light-harvesting" task should then be evaluated by the integrated current as a function of the total absorption (Figure 13). We

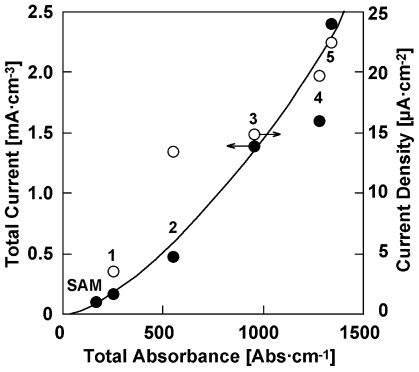


Figure 13. Plots of the photocurrent against the total absorbance at −200 mV (versus Ag/AgCl). The total absorbance was estimated from the integration of the absorption (arbitrary unit) from 350 to 750 nm in wavenumbers ($cm^{-1}$). The total current density on the left-hand axis (●) was calculated from the integration of the current density ($A\,cm^{-2}$) in Figure 11 from 380 to 750 nm in wavenumbers ($cm^{-1}$). The current density on the right-hand axis (○) was obtained by white light irradiation as shown in Figure 10. The numbers in the figure denote the deposition cycles.

obtained the total absorption and current values from the integration of the cross-sectional absorption and current density over the whole wavenumber range. The result from the plot for the total photocurrent shows a good agreement with the photocurrent observed by white light irradiation. The sharp increase of both the total photocurrent and current intensity increases the efficient "light-harvesting" function of the surface-grafted multiporphyrin arrays.

It is generally accepted that the disordered multichromophoric assemblies dissipate photoexcitation energy at structural defects.[21] However, well-ordered arrangements of chromophores can suppress deactivation pathways and conserve the photoexcited energy.[22] For instance, natural photosynthetic systems have developed sophisticated structures for efficient photoenergy conversion. The multiporphyrin array system composed of the dimer unit mimics these systems, since fluorescence is not quenched at all[11a] and efficient long-range hole and/or energy transfer has been confirmed already.[23] The molecular axes of the multiporphyrin array assist hole shift or energy transfer between the outer terminal and the electrode surface, because the outer porphyrin terminal is connected to the electrode through the surface-grafted chain structure.

**The $C_{60}$-terminated antennae system**: The stepwise immobilization technique permits introduction of a wide variety of substituent-appended imidazolylporphyrins to develop redox- and energy-cascade systems for versatile applications. Here, we show a preliminary trial for the $C_{60}$-terminated system on the gold, since $C_{60}$ is an excellent electron acceptor owing to its extremely small reorganization energy.[3d,h] Zn(ImP)–$C_{60}$ showed dramatically efficient quenching (99.7%) of the photoexcited porphyrin by $C_{60}$ compared with Zn(ImP) (Figure 14), indicating the efficient electron-transfer quenching from the excited singlet of the porphyrin ($^1P^*$) to $C_{60}$.

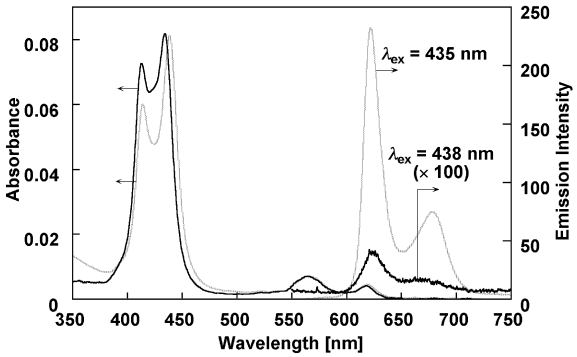


Figure 14. Normalized absorption and emission spectra of Zn(ImP) (thin lines) and Zn(ImP)–$C_{60}$ (thick lines) in $CH_2Cl_2$. The fluorescence spectrum was obtained by excitation at the longer Soret band. The fluorescence of Zn(ImP)–$C_{60}$ is magnified by 100 times.

We soaked the gold surface modified with the multiporphyrin antennae in Zn(ImP)–$C_{60}$ (0.1 mM) and pyridine (2 mM) in $CH_2Cl_2$ for 2 h, followed by treatment with Grubbs catalyst. No significant spectral change in the absorption was found after the treatment of Zn(ImP)–$C_{60}$.[12b] The photocurrent in the $C_{60}$-terminated antennae, however, increased the cathodic photocurrent by approximately three times, in comparison to the case of the unmodified antennae (Figure 15). The enhancement by termination with $C_{60}$

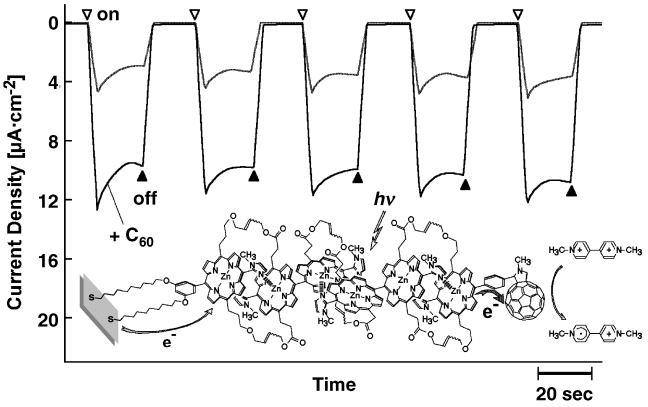


Figure 15. Effect of termination with $C_{60}$ at the multiporphyrin array on the photocurrent response at −200 mV versus Ag/AgCl.

  

should be attributed to the efficient photoinduced charge separation at the array terminal.[3d,i,j] In the antenna system without a $C_{60}$ terminal, the electron-transfer reaction to viologen is assumed to undergo fast intersystem transfer to $^3P^*$ followed by charge separation,[24] which must have been limited by the counter-complex formation with bulk viologen. On the other hand, the $C_{60}$ terminal directly oxidizes $^1P^*$ and efficiently mediates the oxidation of the photoexcited $Zn_2(ImP)_2$ and the electron transfer to bulk viologen. The hole produced migrated to the electrode surface along the multiporphyrin array. The heterodeposition of the imidazolylporphyrins allows construction of the "light-harvesting" system by incorporating a charge-separation unit.

## Conclusions

A surface-grafted multiporphyrin array has been successfully constructed by repetitive coordination cycles of imidazolylporphyrinatozinc and its covalent linkage by ring-closing olefin metathesis of the allyl side chains. The resulting multiporphyrin array will provide a new class of molecular materials. Our results show that this array has dramatically improved light absorption by splitting of absorption bands and an accumulation effect, and thus brought about a significant increase in the photocurrent generation by a so-called "light-harvesting antenna" effect. The photocurrent density was increased by efficient excitation energy/hole-transfer capability even without incorporation of any electron-acceptor or -donor components. Moreover, an electron-acceptor unit could be introduced at the terminal of the multiporphyrin for construction of the redox-cascade system. The sequentially arranged redox system led to a higher efficiency of the electron-transfer reaction, sensitized by the multiporphyrin array at the electrode surface. Further work is in progress to improve the multiporphyrin systems by elaborate modification. This approach will provide an interesting method to improve the small extinction of the molecular assemblies when a flat electrode surface is used.

## Experimental Section

**Synthesis procedures**: Benzylidenebis(tricyclohexylphospine)dichlororuthenium, the Grubbs catalyst, was purchased from Fluka and used without further purification. 1-Octanethiol was dissolved in $CH_2Cl_2$ for adsorption onto the gold surface as-received from TCI.

Imidazolylporphyrins were synthesized from the corresponding aldehydes and dipyrromethane (Scheme 3). The preparation of 2-formyl-1-methylimidazole, dipyrromethanes, and Zn(ImP) is described elsewhere.[14a] All synthesized porphyrins gave satisfactory $^1$H NMR and MALDI-TOF mass spectra. $^1$H NMR spectra were recorded on a JEOL JNMEX 270 or JEOL ECP 600 by using TMS as an internal standard. For the MALDI-TOF MS measurement on a PerSeptive Biosystems Voyager DE-STR, the sample was mixed with dithranol (purchased from Aldrich) as a matrix dye and was put on the gold target plate. UV-visible absorption and emission spectra in isotropic media were measured by using a conventional 1 cm quartz cell under aerobic conditions. The fluorescence spectra were recorded on a HITACHI Fluorescence Spectrometer F-4500.

**5-(1-Methylimidazol-2-yl)-10,20-bis(3-allyloxypropyl)-15-di-3,5-(10-acetylthiodecanoxy)phenylporphyrin ($H_2ImP(C_{10}SAc)_2$)**: The linkage porphyrin was prepared by acid-catalyzed cyclization of a mixture of 2-formyl-1-methylimidazole (45 mg, 1 equiv), di-3,5-(10-acetylthiodecanoxy)benzaldehyde (see Supporting Information) (230 mg, 1 equiv), and 3-allyloxypropyldipyrromethane (198 mg, 2 equiv) in chloroform (74 mL). The mixture was stirred with trifluoroacetic acid (TFA) (0.20 mL, 2 equiv) for 5 h and then oxidized with *p*-chloranil (0.95 g, 3 equiv). The porphyrin $H_2ImP(C_{10}SAc)_2$ was eluted with chloroform/acetone (9:1 v/v) from a silica-gel column (59.6 mg, 4.1 %). $^1$H NMR (600 MHz) in $CDCl_3$: $\delta = -2.65$ (s, 2H; inner proton), 1.25–1.88 (br, 32H; alkyl), 2.28 (s, 6H; $-SCOCH_3$), 2.79 (t, $J = 6.6$ Hz, 4H; $-CH_2CH_2O$-allyl), 2.83 (m, 4H; $-CH_2SCOMe$), 3.40 (s, 3H; N$-CH_3$), 3.66 (t, $J = 4.8$ Hz, 4H; $-CH_2O$-allyl), 4.08 (m, 4H; $-OCH_2CH{=}CH_2$), 4.12 (m, 4H; Ph-$OCH_2-$), 5.10 (t, $J = 7.2$ Hz, 4H; porphyrin-$CH_2(CH_2)_2O$-allyl), 5.23 (dd, $J = 1.8$, 9.6 Hz, 2H; $-CH{=}CHH$), 5.42 (dd, $J = 1.8$, 16.2 Hz, 2H; $-CH{=}CHH$), 6.08 (ddt, $J = 6.0$, 9.6, 16.2 Hz, 2H; $-CH{=}CH_2$), 6.91 (s, 1H; Ph), 7.23 (s, 1H; Ph), 7.39 (s, 1H; Ph), 7.48 (s, 1H; 5-imidazolyl), 7.69 (s, 1H; 4-imidazolyl, 1H), 8.77 (d, $J = 5.4$ Hz, 2H; β-pyrrole), 9.00 (d, $J = 5.4$ Hz, 2H; β-pyrrole), 9.47 (d, $J = 4.8$ Hz, 2H; β-pyrrole), 9.53 ppm (d, $J = 4.8$ Hz, 2H; β-pyrrole); MALDI-TOF MS: $m/z$ calcd: 1122.61; found: 1123.96 $[M+H]^+$; UV/Vis ($CHCl_3$): $\lambda_{max} = 414$, 437, 566, 619 nm.

**5-(1-Methylimidazol-2-yl)-10,20-bis(3-allyloxypropyl)-15-di-3,5-(10-mercaptodecanoxy)phenylporphyrin ($H_2ImP(C_{10}SH)_2$)**: Acetyl-protected thiol groups were deacylated by alkaline hydrolysis. To avoid decomposition under basic conditions, a central zinc atom was introduced into the porphyrin ring of $H_2ImP(C_{10}SAc)_2$ with zinc acetate (yield 90 %). The solution of thioacetyl-terminated porphyrin (27 mg) in chloroform/methanol (10 mL, 4:1 v/v) was treated with potassium hydroxide (0.2 g) in water/methanol (2:3 v/v) at room temperature for 0.5 h. After washing with water, the organic layer was treated with hydrochloric acid to remove the central zinc atom. The mixture was subjected to silica-gel column chromatography to elute $H_2ImP(C_{10}SH)_2$ with chloroform/methanol (10:1 v/v). $^1$H NMR (600 MHz) in $CDCl_3$: $\delta = -2.77$ (s, 2H; inner proton), 0.77–1.81 (br, 32H; alkyl), 2.40 (m, 4H; $-CH_3SH$), 2.71 (m, 4H; $-CH_2CH_2O$-allyl), 3.31 (s, 3H; N$-CH_3$), 3.58 (t, $J = 6.0$ Hz, 4H; $-CH_2O$-allyl), 4.00 (m, 4H; $-OCH_2CH{=}CH_2$), 4.06 (m, 4H; Ph-$OCH_2-$), 5.11 (t, $J = 7.8$ Hz, 4H; porphyrin-$CH_2(CH_2)_2O$-allyl), 5.18 (dd, $J = 1.8$, 10.2 Hz, 2H; $-CH{=}CHH$), 5.34 (dd, $J = 1.8$, 18.0 Hz, 2H; $-CH{=}CHH$), 6.00 (ddt, $J = 6.0$, 10.2, 18.0 Hz, 2H; $-CH{=}CH_2$), 6.83 (s, 1H; Ph), 7.22 (s, 1H; Ph), 7.32 (s, 1H; Ph), 7.39 (s, 1H; 5-imidazolyl), 7.61 (s, 1H; 4-imidazolyl), 8.70 (d, $J = 4.2$ Hz, 2H; β-pyrrole), 8.92 (d, $J = 4.2$ Hz, 2H; β-pyrrole), 9.39 (d, $J = 4.2$ Hz, 2H; β-pyrrole), 9.45 ppm (d, $J = 4.2$ Hz, 2H; β-pyrrole); no peaks were observed with MALDI-TOF MS because the thiol groups were strongly bound to the gold plate. UV/Vis ($CHCl_3$): $\lambda_{max} =$ 419, 516, 554, 590, 648 nm.

**5-(1-Methylimidazol-2-yl)-10,20-bis(2-methoxycarbonylethyl)porphyrinatozinc (Zn(ImPH))**: A mixture of 2-formyl-1-methylimidazole (0.55 g, 1 equiv), paraformaldehyde (0.80 g, 4 equiv), and 2-methoxycarbonylethyldipyrromethane (2.3 g, 2 equiv) in chloroform (500 mL) were mixed with trifluoroacetic acid (0.75 mL, 2 equiv). After oxidation with chloranil (3.7 g, 3 equiv), and neutralization with saturated aq $NaHCO_3$, the desired porphyrin was roughly separated from the byproducts by means of silica-gel column chromatography, followed by introduction of central zinc by treatment with zinc acetate. Column chromatography with chloroform/acetone (5:1 v/v) as eluent, and rinsing with diethyl ether afforded the precursor porphyrin (yield 3 %). $^1$H NMR (270 MHz) in $CDCl_3$: $\delta = 1.59$ (s, 3H; N$-CH_3$, 3H), 1.85 (s, 1H; 5-imidazolyl), 3.87–3.91 (m, 4H; $-CH_2COOMe$), 3.91 (s, 6H; $-COOCH_3$), 5.42 (s, 2H; 3,7-β-pyrrole), 5.44 (s, 1H; 4-imidazolyl), 5.52 (t, $J = 8.6$ Hz, 4H; $-CH_2CH_2COOMe$), 8.95 (d, $J = 4.6$ Hz, 2H; 2, 8-β-pyrrole), 9.54, 9.74 (d, 4H; 4.32 Hz, 12,13,17,18-β-pyrrole), 10.29 ppm (s, 1H; *meso*-porphyrin); MALDI-TOF MS: $m/z$calcd: 624.15; found: 625.35 $[M+H]^+$; UV/Vis ($CHCl_3$): $\lambda_{max} = 408$, 430, 559, 608 nm.

**15,15′-Bis{5-(1-methylimidazol-2-yl)-10,20-bis(2-methoxycarbonylethyl)-porphyrin} ($H_4ImP_2$)**: A solution of the *meso*-free precursor porphyrin

  

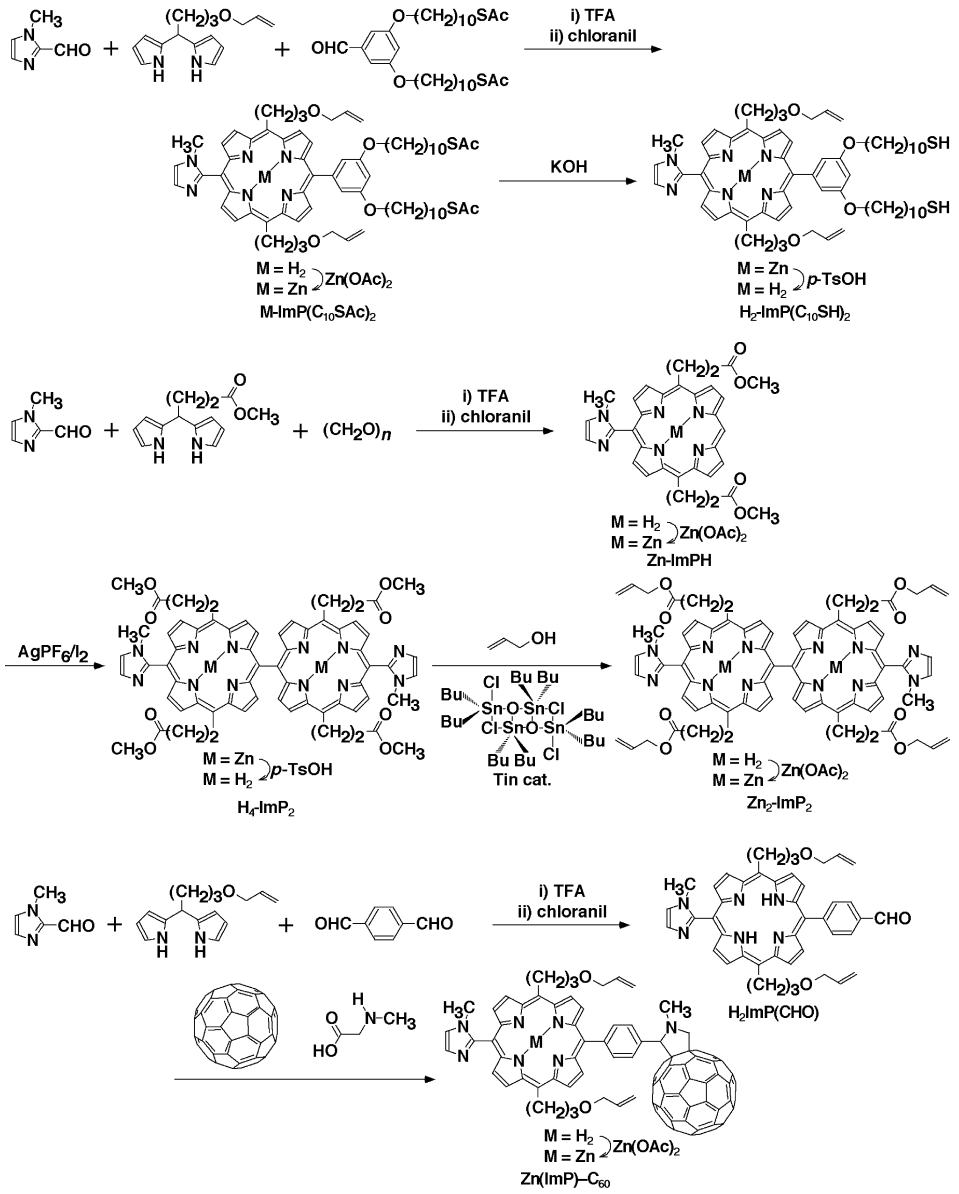


Scheme 3. Synthesis of the imidazolylporphyrins.

Zn(ImPH) (174 mg, 1 equiv) in chloroform (90 mL) was deaerated by nitrogen bubbling. The addition of 0.5 equiv of $AgPF_6$ (47 mg, 0.6 equiv) and $I_2$ (39 mg, 0.5 equiv) promoted a *meso,meso*-coupling reaction.[25] The reaction was quenched within 20 min by adding aqueous sodium thiosulfate (ca. 100 mL). The mixture was then washed with aqueous sodium hydrogencarbonate and brine. The crude product was demetalated with HCl/methanol (10:1 v/v). Free-base *meso,meso*-coupled bisporphyrin ($H_4ImP_2$) was purified by silica-gel column chromatography with chloroform/acetone as eluent (5:1 → 1:1 v/v) (yield 49%). $^1$H NMR (270 MHz) in $CDCl_3$: $\delta = -2.17$ (s, 4H; N*H*), 3.53 (m, 14H; N−C*H*$_3$, −C*H*$_2$COOMe), 3.70 (d, $J = 3.24$ Hz, 6H; −COOC*H*$_3$), 5.33 (m, 8H; −C*H*$_2$CH$_2$COOMe), 7.56 (d, $J = 1.4$ Hz, 2H; 5-imidazolyl), 7.76 (d, $J = 1.4$ Hz, 2H; 4-imidazolyl), 7.99, 8.14 (d, $J = 4.7$ Hz, 4H; 13,13′,17,17′-β-pyrrole), 8.94 (d, $J = 4.1$ Hz, 4H; 4,4′,7,7′-β-pyrrole), 9.14 (dd, $J = 10.8$, 5.1 Hz, 4H; 12,12′,18,18′-β-pyrrole), 9.59 ppm (dd, $J = 2.3$, 3.0 Hz, 4H; 3,3′,9,9′-β-pyrrole); MALDI-TOF MS: *m/z* calcd: 1122.45; found: 1125.85 $[M+H]^+$; UV/Vis ($CHCl_3$): $\lambda_{max} = 423$, 453, 526, 596 nm.

**15,15′-Bis{5-(1-methylimidazol-2-yl)-10,20-bis(2-allyloxycarbonylethyl)-porphyrinatozinc} ($Zn_2(ImP)_2$)**: Allyl groups were introduced into the side chains by transesterification catalyzed with 1,3-dichlorotetrabutyldistannoxane.[26] The free-base bis-imidazolylporphyrin with four methyl ester side chains was gently refluxed in toluene/allylalcohol (10:1 v/v) in the presence of ten equivalents of the tin catalyst for 6 h. After removal of the solvent, the tetraallyl-substituted bis-porphyrin was eluted from a silica-gel column with chloroform/acetone (1:1 v/v) as eluent (yield 51%). $^1$H NMR (270 MHz) in $CDCl_3$: $\delta = -2.16$ (s, 4H; N*H*), 3.53 (m, 14H; N−C*H*$_3$, −C*H*$_2$COO-allyl), 4.63 (m, 8H; −COOC*H*$_2$CH=CH$_2$), 5.14 (m, 4H; −CH=CH*H*), 5.23–5,30 (m, 12H; −CH=C*H*H, porphyrin-C*H*$_2$−), 5.80–5.85 (m, 4H; −C*H*=CH$_2$), 7.57 (s, 2H; 5-imidazolyl), 7.76 (s, 2H; 4-imidazolyl), 7.99, 8.14 (d, 4H; $J = 4.8$ Hz, 13,13′,17,17′-β-pyrrole), 8.94 (d, $J = 4.1$ Hz, 4H; 4,4′,7,7′-β-pyrrole), 9.18 (dd, $J = 10.8$, 5.1 Hz, 4H; 12,12′,18,18′-β-pyrrole), 9.59 ppm (dd, $J = 2.3$, 3.0 Hz, 4H; 3,3′,9,9′-β-pyrrole); MALDI-TOF MS: *m/z* calcd: 1226.51; found: 1227.58 $[M+H]^+$; UV/Vis ($CHCl_3$): $\lambda_{max} = 423$, 453, 526, 596 nm.

  

The central zinc atom was introduced into the free-base bis-porphyrin with zinc acetate. After washing with aqueous sodium hydrogencarbonate and brine, $Zn_2(ImP)_2$ was eluted with chloroform/methanol (10:1 v/v) from a silica-gel column. MALDI-TOF MS: *m/z* calcd: 1350.34; found: 1354.4 $[M+H]^+$;UV/Vis ($CH_2Cl_2$): $\lambda_{max}=407$, 490, 582, 633 nm (see also Figure S1 in the Supporting Information).

**5-(1-Methylimidazol-2-yl)-10,20-bis(3-allyloxypropyl)-15-(*p*-formylphenyl)porphyrin ($H_2$ImP(CHO))**: A catalytic amount of TFA (0.32 mL, 2 equiv) was added to a mixture of 2-formyl-1-methylimidazole (225 mg, 1 equiv), terephthalaldehyde (274 mg, 1 equiv), and 3-allyloxypropyldipyrromethane (1.0 g, 2 equiv) in chloroform (400 mL), followed by stirring for 3 h and further stirring after the addition of chloranil (1.5 g, 3 equiv). Elution over a silica-gel column with chloroform/acetone (1:1 v/v) afforded $H_2$ImP(CHO) (yield 4%). $^1$H NMR (600 MHz) in $CDCl_3$: $\delta=-2.69$ (s, 2H; inner proton), 2.78 (m, 4H; porphyrin-$CH_2CH_2CH_2O-$), 3.31 (s, 3H; N−$CH_3$), 3.66 (t, $J=5.4$ Hz, 4H; −$CH_2$O-allyl), 4.08 (m, 4H; −O$CH_2$CH=$CH_2$), 5.01 (t, $J=7.2$ Hz, 4H; porphyrin-$CH_2$−), 5.26 (dd, $J=1.2$, 10.2 Hz, 2H; −OCH$_2$CH=C*H*H), 5.43 (dd, $J=1.2$, 17.4 Hz, 2H; −OCH$_2$CH=CH*H*), 6.08 (ddt, $J=6.0$, 9.6, 16.2 Hz, 2H; −OCH$_2$C*H*=CH$_2$), 7.49 (s, 1H; 5-imidazolyl), 7.69 (s, 1H; 4-imidazolyl), 8.28 (d, $J=7.2$ Hz, 1H; Ph), 8.31 (t, 3H; Ph), 8.42 (d, $J=7.2$, 1H; Ph), 8.80 (d, $J=5.4$ Hz, 2H; β-pyrrole), 8.81 (d, $J=5.4$ Hz, 2H; β-pyrrole), 9.51 (d, $J=5.4$ Hz, 2H; β-pyrrole), 10.41 ppm (s, 1H; −C*H*O); MALDI-TOF MS: *m/z* calcd: 690.33; found: 691.34 $[M+H]^+$; UV/Vis ($CHCl_3$): $\lambda_{max}=418$, 516, 551, 591 nm.

**5,15-Bis(allyloxypropyl)-10-[4-phenyl-2-(*N*-methyl)fulleropyrrolidinyl]-20-(1-methylimidazol-2-yl)porphyrinatozinc (Zn(ImP)–$C_{60}$)**: A mixture of $H_2$ImP(CHO) (37.5 mg, 1 equiv), fullerene (78.1 mg, 2 equiv), and *N*-methylglycine (96.7 mg, 20 equiv) in toluene was gently refluxed under a nitrogen atmosphere in the dark for 12 h.[27] The reaction mixture was subjected to silica-gel column chromatographic separation. The desired porphyrin–fullerene dyad (32 mg, 41%) was eluted with a gradient solvent system from toluene to chloroform/acetone (9:1 v/v). $^1$H NMR (600 MHz) in $CDCl_3$: $\delta=-2.66$ (s, 2H; inner proton), 2.72 (m, 4H; porphyrin-$CH_2CH_2CH_2O-$), 3.13 (s, 3H; pyrrolidine-N$CH_3$), 3.68 (s, 3H; imidazolyl-N$CH_3$), 3.68 (t, $J=5.4$ Hz, 4H; −$CH_2$O-allyl), 4.05 (br, 4H; −O$CH_2$CH=$CH_2$), 4.43 (d, 1H; pyrrolidine-NC*H*H−), 5.01 (t, 4H; $J=7.2$ Hz, porphyrin-$CH_2$−), 5.11, (d, 1H; pyrrolidine-NCH*H*−), 5.28 (s, 1H; pyrolidine-C*H*N−), 5.26 (dd, $J=16.2$ Hz, 2H; −OCH$_2$CH=C*H*H), 5.34 (dd, $J=16.2$ Hz, 2H; −OCH$_2$CH=CH*H*), 6.01 (br, 2H; −OCH$_2$C*H*=CH$_2$), 7.41 (s, 1H; 5-imidazolyl), 7.60 (s, 1H; 4-imidazolyl), 8.20 (s, 4H; Ph), 8.68 (d, $J=13.8$ Hz, 4H; β-pyrrole), 9.31 (s, 2H; β-pyrrole), 9.45 ppm (s, 2H; β-pyrrole); MALDI-TOF MS: *m/z* calcd: 1437.38; found: 1439.96 $[M+H]^+$; UV/Vis ($CHCl_3$): $\lambda_{max}=419$, 516, 551, 592 nm.

We introduced the central zinc atom by treatment with zinc acetate in chloroform. The organic layer was washed with aqueous sodium hydrogencarbonate, a large excess of water, and brine. Zn(ImP)–$C_{60}$ (yield 90%) was purified over a silica-gel column with chloroform/acetone (9:1 v/v) as eluent. MALDI-TOF MS: *m/z* calcd: 1499.29; found: 1502.77 $[M+H]^+$; UV/Vis ($CHCl_3$): $\lambda_{max}=414$, 439, 566, 620 nm. Very weak emissions were observed around 621 and 675 nm ($\lambda_{ex}=438$ nm); 99.7% of these emissions were quenched relative to those observed for non-fullerene-substituted imidazolylporphyrinatozinc Zn(ImP) (Figure 14).

**Measurements**

**Absorption spectra**: A gold substrate was prepared by a vacuum-deposition technique at $5\times10^{-6}$ Torr; 50 Å thickness of Cr and then 200 Å of Au onto a glass slide (ALVAC, VPC-260). The roughness factor, that is, the mean area per apparent area, was found to be approximately 1.07 estimated from measurements made by non-contact mode atomic force microscopy (AFM, Seiko Instruments SPA400).

The substrates were placed perpendicular to the optical path for the general absorption measurements. The absorption spectra, recorded on a Shimadzu UV-3100PC spectrophotometer, were shown as the change in the absorption with respect to the corresponding bare gold.

**Surface plasmon resonance**: Surface plasmon resonance (SPR) measurements were employed to evaluate the thickness of the porphyrin layers on the gold substrate.[28] The SPR measurements were performed in pure water (18 MΩ cm purified by Milli-Q Labo reagent water system). The total reflectance angles of the modified gold were estimated by Fresnel's fittings using the appropriate dielectric constants, $\varepsilon_{water}=1.793$, $\varepsilon_{organic}=2.25$. The gold substrate coupled with the prism ($\varepsilon_{prism}=2.292$) through the matching oil was equipped with a goniometer in the Kretshmann configuration (Nihon Laser Denshi Co.). The SPR angle of the gold substrate in water was scanned by varying the incident angle of a 670 nm laser and the photodetector. During the measurement, the SPR angle increased, implying a swelling behavior. The stationary SPR angle after a 20 min immersion was used to estimate the thickness of the multiporphyrin array.

**Electrochemical and photocurrent measurements**: Electrochemical and photocurrent measurements were performed in a typical three-electrode configuration connected to a potentiostat (BAS, CV-50W). The gold electrode, as the working-electrode, was mounted at the cell window (diameter 6 mm) and exposed to the aqueous electrolyte solutions. A platinum-wire electrode and a Ag/AgCl (saturated KCl) electrode were employed as the counter and reference electrodes, respectively. Sodium sulfate solution (0.1 M) was used as the supporting electrolyte, except for the alkali desorption experiments, where potassium hydroxide (0.5 M) was used. Potassium ferricyanide (purchased from Nacalai Tesque) was used as a bulk redox probe without further purification. All electrochemical measurements were carried out under deaerated conditions.

The experimental set-up for photocurrent measurements is presented in Figure 16. The three-electrode equipment was placed in a dark box. The electron-carrier methylviologen (10 mM) (1,1′-dimethyl-4,4′-dipyridinium dichloride, purchased from TCI) was added to the electrolyte solution. The photocurrent response was recorded under potentiostatic conditions with exposure to the chopped light under a nitrogen stream. The front side of the gold electrode was irradiated by a 150 W xenon arc lamp (Hamamatsu Photonics, L2274 light source equipped with C7535 power supply and C4251 starter) filtered with an IR cut-off filter (Sigma Koki, HAF-50S-50H) or a monochromator (Shimadzu, SPG-120S). The electrode was placed at a distance of 31 cm from the edge of the lamp housing. The profile of the white light exhibits properties similar to solar light.[5a] The light intensity of the monochromatic light at the electrode surface was monitored with a Si light detector (Advantest, Q8221 equipped with Q82214).

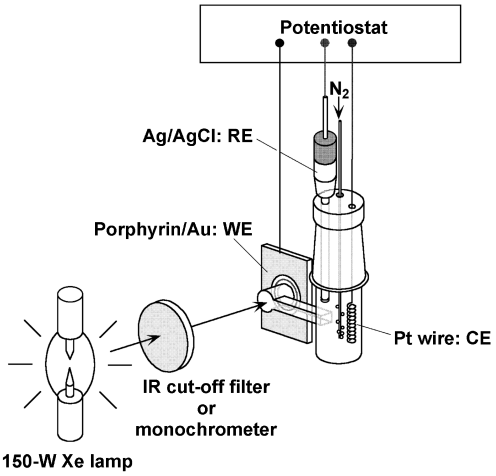


Figure 16. Experimental set-up for the photocurrent measurements.

## Acknowledgements

Y.K. gratefully acknowledges the financial support of CREST (Core Research for Evolutional Science and Technology) program from JST

  

(Japan Science and Technology Agency) and Grant-in-aid for Scientific Research (No. 15205020) from the Ministry of Education, Culture, Sports, Science, and Technology, Japan (Monbu Kagaku Sho).

[1] a) A. Aviram, M. A, Ratner, *Chem. Phys. Lett.* **1974**, *29*, 277; b) R. L. Carroll, C. B. Gorman, *Angew. Chem.* **2002**, *114*, 4556; *Angew. Chem. Int. Ed.* **2002**, *41*, 4378; c) R. M. Metzger, *Chem. Rev.* **2003**, *103*, 3803.

[2] LB film approaches: a) H. Kuhn, D. Möbius, *Angew. Chem.* **1971**, *83*, 672; *Angew. Chem. Int. Ed. Engl.* **1971**, *10*, 620; b) T. Miyasaka, T. Watanabe, A. Fujishima, K. Honda, *J. Am. Chem. Soc.* **1978**, *100*, 6657; c) M. Fujihira, M. Sakomura, T. Kamei, *Thin Solid Films* **1985**, *132*, 77; d) I. Yamazaki, N. Tamai; Yamazaki, A. Murakami, M. Mimuro, Y. Fujita, *J. Phys. Chem.* **1988**, *92*, 5053; e) M. Fujihira, M. Sakomura, T. Kamei, *Thin Solid Films* **1989**, *180*, 43; f) T. Yamazaki, I. Yamazaki, A. Osuka, *J. Phys. Chem. B* **1998**, *102*, 7858; g) B. Choudhury, A. C. Weeden, J. R. Bolton, *Langmuir* **1998**, *14*, 6199; h) A. Aoki, Y. Abe, T. Miyashita, *Langmuir* **1999**, *15*, 1463.

[3] SAM approaches: a) T. Kondo, T. Ito, S. Nomura, K. Uosaki, *Thin Solid Films* **1996**, *284–285*, 652; b) K. Uosaki, T. Kondo, X.-Q. Zhang, M. Yanagida, *J. Am. Chem. Soc.* **1997**, *119*, 8367; c) H. Imahori, H. Norieda, S. Ozawa, K. Ushida, H. Yamada, T. Azuma, K. Tamaki, Y. Sakata, *Langmuir* **1998**, *14*, 5335; d) H. Imahori, H. Norieda, Y. Nisimura, I. Yamazaki, K. Higuchi, N. Kato, T. Motohiro, H. Yamada, K. Tamaki, M. Arimura, Y. Sakata, *J. Phys. Chem. B* **2000**, *104*, 1253; e) H. Imahori, H. Yamada, Y. Nisimura, I. Yamazaki, Y. Sakata, *J. Phys. Chem. B* **2000**, *104*, 2099; f) T. Morita, S. Kimura, S. Kobayashi, Y. Imanishi, *Chem. Lett.* **2000**, 676; T. Morita, S. Kimura, S. Kobayashi, Y. Imanishi, *J. Am. Chem. Soc.* **2000**, *122*, 2850; g) H. Imahori, T. Hasobe, H. Yamada, Y. Nisimura, I. Yamazaki, S. Fukuzumi, *Langmuir* **2001**, *17*, 4925; h) H. Imahori, H. Norieda, H. Yamada, Y. Nisimura, I. Yamazaki, Y. Sakata, S. Fukuzumi, *J. Am. Chem. Soc.* **2001**, *123*, 100; i) D. Hirayama, K. Takiyama, Y. Aso, T. Otsubo, T. Hasobe, H. Yamada, H. Imahori, S. Fukuzumi, Y. Sakata, *J. Am. Chem. Soc.* **2002**, *124*, 532; j) H. Yamada, H. Imahori, Y. Nishimura, I. Yamazaki, T.-K. Ahn, S.-K. Kim, D. Kim, S. Fukuzumi, *J. Am. Chem. Soc.* **2003**, *125*, 9129; k) T. Hasobe, H. Imahori, H. Yamada, T. Sato, K. Ohkubo, S. Fukuzumi, *Nano Lett.* **2003**, *3*, 409.

[4] Layer-by-layer approaches: a) K. Araki, M. J. Wagner, M. S. Wrighton, *Langmuir* **1996**, *12*, 5393; b) K. Ariga, Y. Lvov, T. Kunitake, *J. Am. Chem. Soc.* **1997**, *119*, 2224; c) M. Lahav, T. Gabriel, A. N. Shipway, I. Willner, *J. Am. Chem. Soc.* **1999**, *121*, 258; d) A. Ikeda, T. Hatano, S. Shinkai, T. Akiyama, S. Yamada, *J. Am. Chem. Soc.* **2001**, *123*, 4855; e) F. B. Abdelrazzaq, R. C. Kwong, M. E. Thompson, *J. Am. Chem. Soc.* **2002**, *124*, 4796; f) D.-J. Qian, C. Nakamura, T. Ishida, S.-O. Wenk, T. Wakayama, S. Takeda, J. Miyake, *Langmuir* **2002**, *18*, 10237.

[5] a) M. K. Nazeeruddin, A. Kay, I. Rodicio, R. Humphry-Baker, E. Müller, P. Liska, N. Vlachopoulos, M. Grätzel, *J. Am. Chem. Soc.* **1993**, *115*, 6382; b) A. Hagfeldt, M. Grätzel, *Chem. Rev.* **1995**, *95*, 49.

[6] Metal–ligand approaches: a) A. Hatzor, T. Moav, H. Cohen, S. Matlis, J. Libman, A. Vaskevich, A. Shanzer, I. Rubinstein, *J. Am. Chem. Soc.* **1998**, *120*, 13469; A. Hatzor, T. Boom-Moav, S. Yochelis, A. Vaskevich, A. Shanzer, I. Rubinstein, *Langmuir* **2000**, *16*, 4420; b) M. A. Ansell, A. C. Zeppenfeld, K. Yoshino, E. B. Cogan, C. J. Page, *Chem. Mater.* **1996**, *8*, 591; c) M. Maskus, H. D. Abruña, *Langmuir* **1996**, *12*, 4455; d) D. L. Thimsen III, T. Phyly-Bobin, F. Papadimitrakopoulos, *J. Am. Chem. Soc.* **1998**, *120*, 6177.

[7] a) G. McDermott, S. M. Prince, A. A. Freer, A. M. Hawthornthwaite-Lawless, M. Z. Papiz, R. J. Cogdell, N. W. Isaacs, *Nature* **1995**, *374*, 517; b) T. Pullerits, V. Sundström, *Acc. Chem. Res.* **1996**, *29*, 381.

[8] Metalloporphyrin–ligand approaches: a) D.-Q. Li, L. W. Moore, B. I. Swanson, *Langmuir* **1994**, *10*, 1177; b) D. A. Offord, S. B. Sachs, M. S. Ennis, T. A. Eberspacher, J. H. Griffin, C. E. D. Chidsey, J. P. Collman, *J. Am. Chem. Soc.* **1998**, *120*, 4478; c) G. Ashkenasy, J. Libman, G. Rubinstein, A. Shanzer, *Angew. Chem.* **1999**, *111*, 1333; *Angew. Chem. Int. Ed.* **1999**, *38*, 1257; G. Kalyuzhny, A. Vaskevich, G. Ashkenasy, A. Shanzer, I. Rubinstein, *J. Phys. Chem. B* **2000**, *104*, 8238; d) S. Zou, R. S. Clegg, F. C. Anson, *Langmuir* **2002**, *18*, 3241; e) T. A. Eberspacher, J. P. Collman, C. E. D. Chidsey, D. L. Donohue, H. Van Ryswyk, *Langmuir* **2003**, *19*, 3814.

[9] Y. Kobuke, H. Miyaji, *J. Am. Chem. Soc.* **1994**, *116*, 4111; Y. Kobuke, H. Miyaji, *Bull. Chem. Soc. Jpn.* **1996**, *69*, 3563.

[10] R. Takahashi, Y. Kobuke, *J. Am. Chem. Soc.* **2003**, *125*, 2372.

[11] a) K. Ogawa, Y. Kobuke, *Angew. Chem.* **2000**, *112*, 4236; K. Ogawa, Y. Kobuke, *Angew. Chem. Int. Ed.* **2000**, *39*, 4070; b) K. Ogawa, T. Zhang, K. Yoshihara, Y. Kobuke, *J. Am. Chem. Soc.* **2002**, *124*, 22; c) C. Ikeda, E. Fujiwara, A. Satake, Y. Kobuke, *Chem. Commun.* **2003**, 616; d) K. Ogawa, A. Ohashi, Y. Kobuke, K. Kamada, K. Ohta, *J. Am. Chem. Soc.* **2003**, *125*, 13356.

[12] a) A. Nomoto, Y. Kobuke, *Chem. Commun.* **2002**, 1104; b) A. Nomoto, H. Mitsuoka, H. Ozeki, Y. Kobuke, *Chem. Commun.* **2003**, 1075.

[13] a) E. L. Dias, S. T. Nguyen, R. H. Grubbs, *J. Am. Chem. Soc.* **1997**, *119*, 3887; b) T. M. Trnka, R. H. Grubbs, *Acc. Chem. Res.* **2001**, *34*, 18.

[14] a) A. Ohashi, A. Satake, Y. Kobuke, *Bull. Chem. Soc. Jpn.* **2004**, *77*, 365; b) C. Ikeda, A. Satake, Y. Kobuke, *Org. Lett.* **2003**, *5*, 4935.

[15] a) C. A. Widrig, C. Chung, M. D. Porter, *J. Electroanal. Chem. Interfacial Electochem.* **1991**, *310*, 335; b) M. M. Walczak, D. D. Popenoe, R. S. Deinhammer, B. D. Lamp, C. Chung, M. D. Porter, *Langmuir* **1991**, *7*, 2687.

[16] M. D. Porter, T. B. Bright, D. L. Allara, C. E. D. Chidsey, *J. Am. Chem. Soc.* **1987**, *109*, 3559.

[17] M. Weck, J. J. Jackiw, R. R. Rossi, P. S. Weiss, R. H. Grubbs, *J. Am. Chem. Soc.* **1999**, *121*, 4088.

[18] S. Ohshima, T. Kajiwara, M. Hiramoto, K. Hashimoto, T. Sakata, *J. Phys. Chem.* **1986**, *90*, 4474.

[19] a) F. J. Kampas, M. Gouterman, *J. Phys. Chem.* **1977**, *81*, 690; b) F. J. Kampas, K. Yamashita, J. Fajer, *Nature* **1980**, *284*, 40; c) Y. Harima, K. Yamashita, *J. Phys. Chem.* **1985**, *89*, 5325; d) H. Yanagi, M. Ashida, Y. Harima, K. Yamashita, *Chem. Lett.* **1990**, 385.

[20] a) R. Dabestani, A. J. Bard, A. Campion, M. A. Fox, T. E. Mallouk, S. E. Webber, J. M. White, *J. Phys. Chem.* **1988**, *92*, 1872; b) N. Vlachopoulos, P. Liska, J. Augustynski, M. Grätzel, *J. Am. Chem. Soc.* **1988**, *110*, 1216; c) I. Bedja, P. V. Kamat, X. Hua, A. G. Lappin, S. Hotchandani, *Langmuir* **1997**, *13*, 2398; d) F. Fungo, L. Otero, C. D. Borsarelli, E. N. Durantini, J. J. Silber, L. Sereno, *J. Phys. Chem. B* **2002**, *106*, 4070.

[21] a) W. Klöpffer, *J. Chem. Phys.* **1969**, *50*, 2337; b) H. Nakamura, H. Fujii, H. Sakaguchi, T. Matsuo, N. Nakashima, K. Yoshihara, T. Ikeda, S. Tazuke, *J. Phys. Chem.* **1988**, *92*, 6151.

[22] a) A. Nakano, T. Yamazaki, Y. Nishimura, I. Yamazaki, A. Osuka, *Chem. Eur. J.* **2000**, *6*, 3254; b) N. Aratani, H. S. Cho, T. K. Ahn, S. Cho, D. Kim, H. Sumi, A. Osuka, *J. Am. Chem. Soc.* **2003**, *125*, 9668; c) D. H. Yoon, S. B. Lee, K.-H. Yoo, J. Kim, J. K. Lim, N. Aratani, A. Tsuda, A. Osuka, D. Kim, *J. Am. Chem. Soc.* **2003**, *125*, 11062.

[23] D. Furutsu, A. Satake, Y. Kobuke, *Inorg. Chem.* **2005**, *44*, 4460.

[24] a) K. Kalyanasundaram, M. Neumann-Spallart, *J. Phys. Chem.* **1982**, *86*, 5163; b) T. Nagamura, N. Takeyama, K. Tanaka, T. Matsuo, *J. Phys. Chem.* **1986**, *90*, 2247; c) A. Uehata, H. Nakamura, S. Usui, T. Matsuo, *J. Phys. Chem.* **1989**, *93*, 8197.

[25] A. Osuka, H. Shimidzu, *Angew. Chem.* **1997**, *109*, 93; *Angew. Chem. Int. Ed. Engl.* **1997**, *35*, 135.

[26] J. Otera, N. Dan-oh, H. Nozaki, *J. Org. Chem.* **1991**, *56*, 5307.

[27] a) M. Maggini, G. Scorrano, M. Prato, *J. Am. Chem. Soc.* **1993**, *115*, 9798; b) T. D. Ros, M. Prato, F. Novello, M. Maggini, E. Banfi, *J. Org. Chem.* **1996**, *61*, 9070.

[28] K. Kobayashi, S. Imabayashi, K. Fujita, K. Nonaka, T. Kakiuchi, H. Sasabe, W. Knoll, *Bull. Chem. Soc. Jpn.* **2000**, *73*, 1993.

Received: January 14, 2005
Published online: July 12, 2005

  